2010

PROGRESSIVE STAR FORMATION IN THE YOUNG GALACTIC SUPER STAR CLUSTER NGC 3603

G Beccari

L Spezzi

G De Marchi

F Parseces

E Young

See next page for additional authors

Authors

G Beccari, L Spezzi, G De Marchi, F Parseces, E Young, M Andersen, N Panagia, B Balick, and D Calzetti

PROGRESSIVE STAR FORMATION IN THE YOUNG GALACTIC SUPER STAR CLUSTER NGC 3603

Giacomo Beccari[1], Loredana Spezzi[1], Guido De Marchi[1], Francesco Paresce[2], Erick Young[3], Morten Andersen[1], Nino Panagia[4,5,6], Bruce Balick[7], Howard Bond[4], Daniela Calzetti[8], C. Marcella Carollo[9], Michael J. Disney[10], Michael A. Dopita[11], Jay A. Frogel[12], Donald N. B. Hall[13], Jon A. Holtzman[14], Randy A. Kimble[15], Patrick J. McCarthy[16], Robert W. O'Connell[17], Abhijit Saha[18], Joseph I. Silk[19], John T. Trauger[20], Alistair R. Walker[21], Bradley C. Whitmore[4], Rogier A. Windhorst[22]

Accepted for publication in The Astrophysical Journal

ABSTRACT

Early release science observations of the cluster NGC3603 with the WFC3 on the refurbished HST allow us to study its recent star formation history. Our analysis focuses on stars with Hα excess emission, a robust indicator of their pre-main sequence (PMS) accreting status. The comparison with theoretical PMS isochrones shows that 2/3 of the objects with Hα excess emission have ages from 1 to 10 Myr, with a median value of 3 Myr, while a surprising 1/3 of them are older than 10 Myr. The study of the spatial distribution of these PMS stars allows us to confirm their cluster membership and to statistically separate them from field stars. This result establishes unambiguously for the first time that star formation in and around the cluster has been ongoing for at least 10-20 Myr, at an apparently increasing rate.

Subject headings: stars: pre-main sequence - open clusters and associations: individual (NGC 3603)

1. INTRODUCTION

The galactic giant HII region NGC 3603 located at a distance of 7 ± 1 kpc (Moffat 1983) is part of the RCW 57 complex SE of Eta Car in the Carina arm. The young, bright, compact stellar cluster (HD97950 or NGC 3603YC) lies at the core of this region and has long been the center of attention for the relatively numerous population of massive stars at its center. The collection of 3 WNL, 6 O3 and numerous late O type

stars together with a bolometric luminosity of 100 times that of the Orion cluster and 0.1 times that of NGC 2070 in the 30 Dor complex in the Large Magellanic Cloud (LMC) and a total mass in excess of $10^4 M_\odot$ (Harayama et al. 2008, hereafter HA08, and references therein) places it squarely in the category of a super star cluster of the type more commonly seen in star burst regions of young galaxies. Thus, it represents a resolved possible prototype of the building blocks of forming or merging galaxies (Larsen 2009) and an excellent opportunity to better understand their complex star formation history and the physical processes involved (see, for example, Peters et al. 2010; Moeckel & Bate 2010; Portegies Zwart et al. 2010).

In this context, NGC 3603YC (from now on referred to as simply NGC 3603) certainly contains many stars younger than 3 Myr but it is so far unclear if it also contains older stars as might be suggested by the presence in the field of the evolved star Sher 25 (Melena et al. 2008), located $\sim 20''$ north to the cluster center. This exciting possibility has yet to be established unambiguously because the latter's membership in the cluster is still quite uncertain. The determination of the cluster's initial mass function (IMF), of course, also depends critically on its formation history as imprinted in the age distribution that can only be determined accurately once we disentangle the various populations from each other. Results on this cluster's IMF (HA08; Stolte et al. 2006; Sung & Bessell 2004) may be affected by imperfect correction for this effect.

In order to investigate the star formation history in NGC 3603, we have used the Wide Field Camera 3 (WFC3) on Hubble Space Telescope (HST) in the UVIS mode to image NGC 3603 with broad band and narrow band filters as part of the early release science (ERS) program. In this paper, we describe the first results of this investigation. The observations and analysis procedure are presented in Section 2. In Section 3 we show the resulting color magnitude diagram (CMD) and the estimation of field contamination and extinction. In Section 4 we describe the identification of pre-Main Sequence (PMS) stars, while their spatial distribution and a discussion of the preliminary physical implications of the results can be found in Section 5 and 6, respectively.

[1] ESA, Space Science Department, Keplerlaan 1, 2200 AG Noordwijk, The Netherlands

[2] INAF - Istituto di Astrofisica Spaziale e Fisica Cosmica, via P. Gobetti, 101, I-40129 Bologna, Italy

[3] NASA–Ames Research Center, Moffett Field, CA 94035

[4] Space Telescope Science Institute, Baltimore, MD 21218, USA

[5] INAF-CT, Osservatorio Astrofisico di Catania, Via S. Sofia 78, 95123 Catania, Italy

[6] Supernova Ltd, OYV #131, Northsound Road, Virgin Gorda, British Virgin Islands

[7] Dept. of Astronomy, University of Washington, Seattle, WA 98195-1580, USA

[8] Dept. of Astronomy, University of Massachusetts, Amherst, MA 01003, USA

[9] Department of Physics, ETH-Zurich, Zurich, 8093 Switzerland

[10] School of Physics and Astronomy, Cardiff University, Cardiff CF24 3AA, United Kingdom

[11] Research School of Astronomy & Astrophysics, The Australian National University, ACT 2611, Australia

[12] Association of Universities for Research in Astronomy, Washington, DC 20005

[13] Institute for Astronomy, University of Hawaii, Honolulu, HI 96822

[14] Department of Astronomy, New Mexico State University, Las Cruces, NM 88003

[15] NASA–Goddard Space Flight Center, Greenbelt, MD 20771

[16] Observatories of the Carnegie Institution of Washington, Pasadena, CA 91101-1292

[17] Department of Astronomy, University of Virginia, Charlottesville, VA 22904-4325

[18] National Optical Astronomy Observatories, Tucson, AZ 85726-6732

[19] Department of Physics, University of Oxford, Oxford OX1 3PU, United Kingdom

[20] NASA–Jet Propulsion Laboratory, Pasadena, CA 91109

[21] Cerro Tololo Inter-American Observatory, La Serena, Chile

[22] School of Earth and Space Exploration, Arizona State University, Tempe, AZ 85287-1404
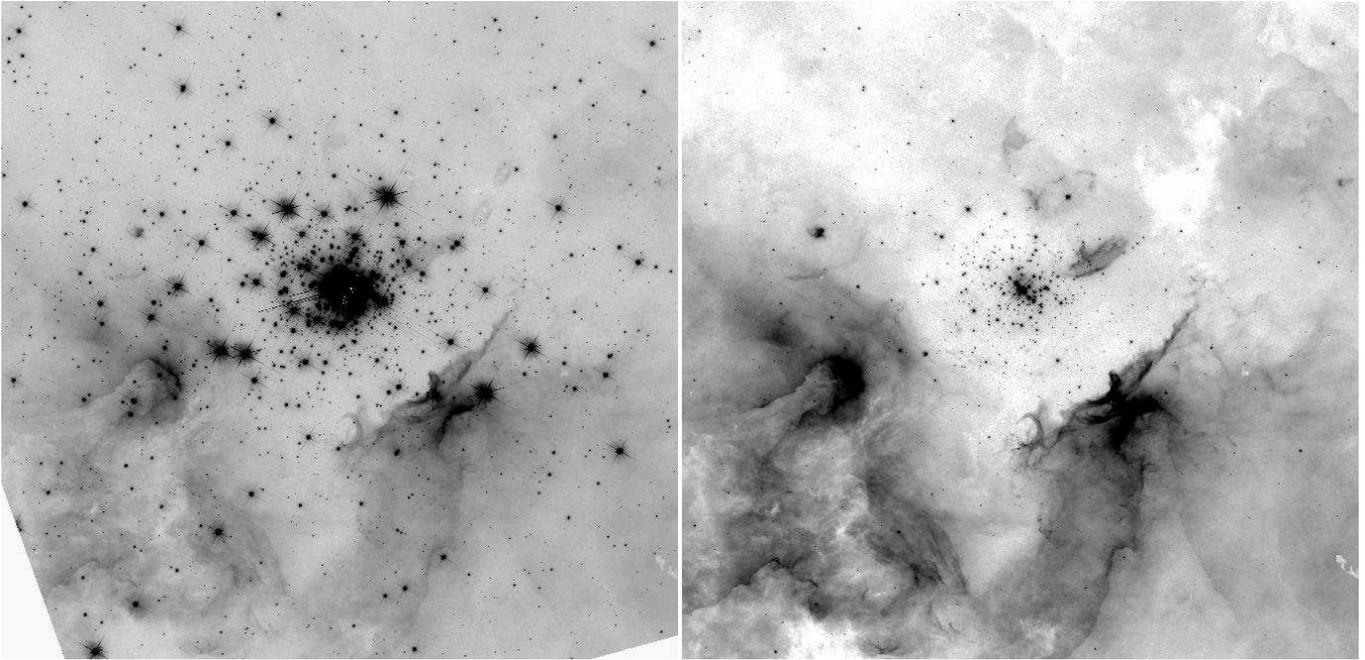
FIG. 1.— WFC3 $2'.2 \times 2'.2$ mosaic images in the $F555W$ (left panel) and $F656N$ (Hα line; right panel) filters of NGC 3603 star forming region as obtained through PyRAF/MULTIDRIZZLE package. North is 30° to the right of the vertical. East is to the left of North.

2. OBSERVATIONS AND DATA REDUCTION

The photometric data used in this work consist of a series of deep multi-band images acquired with the new WFC3 on board of the HST. The WFC3 consists of two detectors, one optimized for observations in the wavelength range ~ 200 to ~ 1000 nm (UVIS channel) and the other between ~ 0.9 and ~ 1.7 μm (IR channel). The UVIS detector consists of two 2Kx4K CCDs covering a field of view (FoV) of $162''$x $162''$ at a plate scale of $0''.04$/px. The IR detector is a single 1Kx1K HgCdTe CCD offering a total FoV of $123''$x $136''$ at a pixel resolution of $0''.13$. A more detailed description of the WFC3 and its current performances can be found in Wong et al. (2010).

The data used in this work are part of the ERS observations[23] obtained by the WFC3 Scientific Oversight Committee for the study of star forming regions in nearby galaxies (Program ID number 11360). NGC 3603 was observed using both the UVIS and IR channels. In this paper we use the images taken through the broad-band $F555W$ and $F814W$ and narrow-band $F656N$ filters for a total exposure time of 1000s, 1550s and 990s, respectively. The IR data-set will be presented in a separate paper (Spezzi et al. 2010, in preparation).

Three images with approximately the same exposure times were taken with a few pixel dithering in order to allow for the removal of cosmic rays, hot pixels and other detector blemishes. All the observations were performed so that the core of NGC 3603 is roughly at the center of the camera's FoV. In Figure 1 we show a mosaic of the images in the $F555W$ (left panel) and $F656N$ (right panel) filters as obtained with the PyRAF/MULTIDRIZZLE package.

The photometric analysis of the entire data-set was performed on the flat-fielded (FLT) images by adopting the following strategy. The images, corrected for bias and flatfield, need a further field-dependent correction factor to achieve uniformity in the measured counts of an object across the field. Applying the correction simply involves multiplying the FLT images by the pixel area map images. A large number of isolated, well exposed stars were selected in every image over the entire FoV in order to properly model the point spread function (PSF) with the DAOPHOTII/PSF routine (Stetson 1987). We used a Gaussian analytic function and a second order look-up table was necessary in order to properly account for the spatial variation in the images.

A first list of stars was generated by searching for objects above the 3σ detection limit in each individual image and a preliminary PSF fitting run was performed using DAOPHOTII/ALLSTAR. We then used DAOMATCH and DAOMASTER to match all stars in each chip, regardless of the filter, in order to get an accurate coordinate transformation between the frames. A master star list was created using stars detected in the $F814W$ band (the deepest in the UVIS data-set) with the requirement that a star had to be detected in at least two of the three images in this filter.

We used the sharpness (sh) and chi square parameters given by ALLSTAR in order to remove spurious detections. It has already been shown (see e.g. Cool et al. 1996; Ascenso et al. 2007) that these parameters are good tracers of the photometric quality. By using a sample of real stars we found the range $-0.15 < sh < 0.15$ to be safe enough to eliminate most spurious objects. The final catalogue was then obtained by rejecting any residual spurious source (mostly associated with bright emission peaks in the HII region not due to point sources) through visual inspection of the drizzled images. The master list was then used as input for ALLFRAME (Stetson 1994), which simultaneously determines the brightness of the stars in all frames while enforcing one set of centroids and one transformation between all images. All the magnitudes for each star were normalized to a reference frame and averaged together, and the photometric error was derived as the standard deviation of the repeated measurements. The final catalogue of the UVIS $F555W$, $F656N$ and $F814W$ bands

---

[23] A complete description of the program, targets and the observations can be found at the web page http://archive.stsci.edu/prepds/wfc3ers/
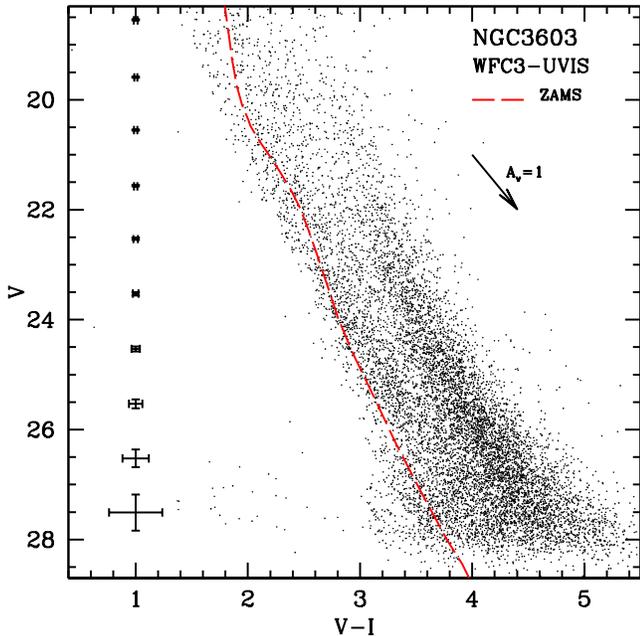
FIG. 2.— Color magnitude diagram of NGC 3603 as obtained from WFC3 observations. The ZAMS from Marigo et al. (2008) at the solar metallicity for an assumed distance modulus $(m-M)_0 = 13.9$ and average extinction $A_V = 4.5$ is over-plotted (dashed line). The average photometric magnitudes and color errors are shown (crosses). The reddening vector (Av=1) is also shown.

contains around 10,000 stars.

The photometric calibration was performed following Kalirai et al. (2009). A sample of bright isolated stars was used to transform the instrumental magnitudes to a fixed aperture of $0.''4$. The magnitudes were then transformed into the VEGAMAG system by adopting the synthetic zero points for the UVIS bands (see Table 5 of Kalirai et al. 2009). Hereafter we will refer to the calibrated magnitudes as V, I , and Hα to indicate m_{F555W}, m_{F814W} and m_{F656N}, respectively.

The WFC3/UVIS channel is affected by geometric distortion and a correction is necessary in order to properly derive the absolute positions of individual stars in each catalogue. We used the distortion coefficients derived by Kozhurina-Platais et al. (2009) to obtain relative star positions that are corrected for distortion. We then used the stars in common between our UVIS and the 2MASS catalogues to derive an astrometric solution and obtain the absolute RA and DEC positions of our stars. We find a systematic residual of $\sim 0.''3$ with respect to the 2MASS coordinates.

3. THE UVIS COLOR MAGNITUDE DIAGRAM

The CMD as obtained with our photometric reduction procedure is shown in Figure 2. Typical photometric errors (magnitudes and colors) are indicated by black crosses. This is the deepest and most accurate optical diagram derived so far for this cluster, demonstrating the unprecedented photometric capabilities and the resolving power of the new WFC3. We show in the CMD the position of the zero age MS (ZAMS) from Marigo et al. (2008) for solar metallicity (solid line), having adopted a distance modulus $(m-M)_0 = 13.9$ (see HA08 and references therein), the average value of the extinction $A_V = 4.5$ as reported in the literature (see Sung & Bessell 2004, hereafter SB04), and having assumed the extinction law of Cardelli et al. (1989). Note that the value of $A_V = 4.5$ is assumed here only for illustration purposes and for comparison

with previous studies, as we will show later that the actual extinction value is larger in the area that we studied. Nonetheless, the position of the ZAMS obtained in this way helps us to identify a population of candidate MS stars that extend from the saturation limit at $V \simeq 17$ down to $V \simeq 26$. As we will show in Section 3.1 and 3.2, most of these objects are likely foreground field stars but some of them represent a bona-fide low mass MS population belonging to the cluster.

A discontinuity in the stellar color distribution in this CMD separates a population of objects along the ZAMS from one clearly grouped at redder colors and consistent with the young population of PMS stars already detected in NGC 3603 (see e.g. HA08; SB04). This confirms that NGC 3603 is an active star forming region. In order to learn more about the properties of this recent star formation episode, it is useful to compare our CMD with PMS isochrones. However, this requires detailed knowledge of possible sources of error such as the contamination from field stars and the presence of differential reddening. We address these issue here below.

3.1. Field star contamination and extinction

As already discussed by HA08 and Nürnberger & Petr-Gotzens (2002), the region of the CMD fitted by the ZAMS in our CMD is contaminated by field stars with a luminosity distribution roughly in agreement with Galactic models. In order to quantify the degree of contamination, we generated a simulated catalogue of field stars using the Galactic model of Robin et al. (2003). The catalogue covers a projected area of $162'' \times 162''$, corresponding to the FoV of the WFC3 (see Section 2), with a diffuse extinction of 0.7 mag/kpc in a distance interval of 7 kpc (i.e. the cluster distance, see Section 1). Since the magnitudes of the synthetic stars are given in the Johnson-Cousins (JC) photometric system, we used model atmospheres from the ATLAS9 library of Kurucz (1993) to calculate the magnitude difference between the JC and WFC3 photometric systems as a function of the effective temperature of the stars. Comparison of the synthetic catalogue with our CMD reveals that about 85% of the stars in the region around the ZAMS in our photometry are potentially field stars, while it decreases to a few percentage towards the region populated by PMS stars.

Recently, Rochau et al. (2010) presented a proper motion study of NGC 3603 based on HST/WFPC2 (Wide Field Planetary Camera 2) observations obtained ten years apart, respectively in 1997 and 2007. On the left panel of their Figure 2 these authors show the position of field stars (open circles) on the CMD obtained with the Planetary Camera (PC) data. By comparing this diagram with the same obtained when considering only bona-fide cluster members (i.e. those with a similar proper motion; central panel on the same figure), we quantify the field contamination along the MS in the PC data to be of order 50%. Although not explicitly stated in their paper, also Brandl et al. (1999) reach a similar conclusion, as about 50 % of the stars on their original lower MS are still present after statistical subtraction of a comparison field (see their Figure 2). Considering that both the PC dataset used by Rochau et al. (2010) and the observations of Brandl et al. (1999) sample the core region of the cluster, where the density of cluster stars is highest, we conclude that the 85 % value of field star contamination that we find in the external regions from the models of Robin et al. (2003) is reasonable and might actually be an overestimate of the true value. We therefore assume it as an upper limit to the contamination level in this field. We will return in Section 3.2 to the work of

Rochau et al. (2010) and Brandl et al. (1999) to discuss their implications for the study of the cluster's stellar population, but we first need to address the issue of differential extinction in this field.

An efficient method to quantify the amount of differential extinction in a star cluster is to use the position of a star in the observed CMD to calculate its distance from a fiducial line (e.g. the ZAMS itself) along the direction of the reddening vector. This distance would be the resultant of two components, namely E(V-I) on the abscissa and A_V on the ordinate, and would give us an estimate of the extinction toward the star itself (see an example in Piotto et al. 1999).

This method works under the assumption that the observed stars are at the same distance, i.e. belong to the same system. As discussed above, the field star contamination in the range of magnitudes covered by our data is high. The described method can be applied in a reliable way only to bright objects (V< 17), since these are very likely cluster members and field star contamination is minimized at these magnitudes. Although our data cannot be used for this purpose, since all stars brighter than $V \sim 17.5$ are saturated, using shorter exposures SB04 were able to perform a study of differential reddening in NGC 3603 taking advantage of multi-band HST photometry of the bright massive stars (i.e. the same objects that are saturated in our images). These authors were able to map the variation of E(B-V) as a function of the distance from the cluster centre (see their Figure 5b). They found that the value $A_V \simeq 4.5$ is representative of the very centre of the OB stars association, while they noticed an increase toward the external regions. Following the work of SB04 and adopting $R_V = 3.55$ as they suggest, we estimate that the mean value of A_V in the area sampled by our observations (from $\sim 10''$ to $\sim 70''$) is $A_V = 5.5$. Therefore, in the rest of this paper we will adopt this value to correct our magnitudes for extinction. The final CMD corrected in this way is shown in Figure 3.

3.2. *The PMS population in NGC 3603*

Once extinction is taken into account, the CMD shown in Figure 3 can be used to determine stellar ages through PMS isochrone fitting. PMS isochrones with ages of 1, 2, 3, 10, 20 and 30 Myr from Siess et al. (2000) are shown in the figure from right to left. We used the same value of the distance modulus adopted for the ZAMS fit. Note that the Siess et al. (2000) models are not available for the WFC3 photometric system. As above, we used the ATLAS9 library of Kurucz (1993) to calculate the magnitude differences between the JC to WFC3 photometric systems. After this correction, the models indicate that the lowest mass that we reach for PMS stars is 0.3 M$_\odot$.

In the magnitude range $V < 20$, where the photometric uncertainty on the $V-I$ color (~ 0.05) is smaller than the typical isochrone separation, the CMD suggests for our PMS stars an age in the range from 1 to 10 Myr, with an average age of 3 Myr. Assuming the PMS isochrones are correct, this can already be considered as tentative evidence of an age spread in the stellar population of NGC 3603.

Recently, HA08 studied the IMF of NGC 3603 using near-infrared (IR) imaging from ground-based adaptive optics photometry of the cluster center obtained with the NAOS–CONICA (NACO) camera and the wider field Infrared Spectrometer and Array Camera (ISAAC) at the Very Large Telescope (VLT). Their $JHKL'$ bands photometry reaches the magnitude limit $J \sim 20.5$ (i.e. $\sim 0.4 M_\odot$ for cluster stars) in an area of $\sim 110''$ radius from the cluster center. By com-
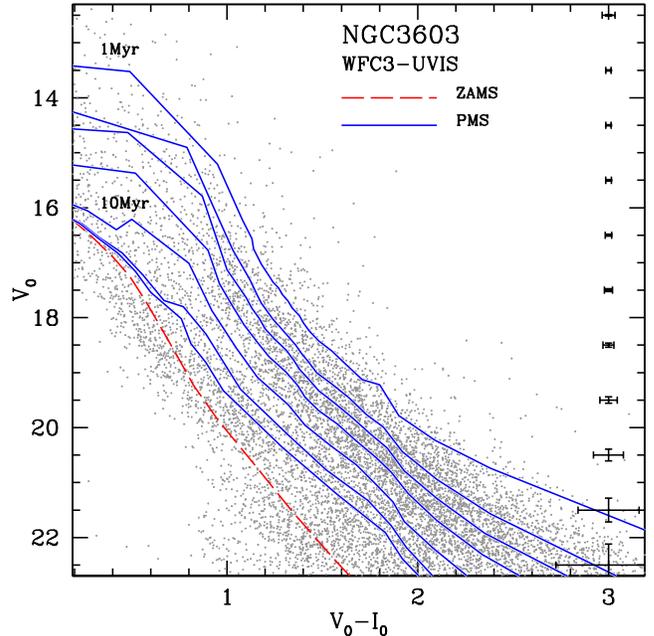

FIG. 3.— De-reddened CMD. The ZAMS from (Marigo et al. 2008, dashed line) is used to identify the location of MS stars. The population of PMS stars is fitted with 1, 2, 3, 5, 10, 20 and 30 Myr PMS isochrones (from right to the left) from Siess et al. (2000) (solid lines). The position of the 1 and 10 Myr isochrones is indicated. According to the models a mass of $M \sim 0.3 M_\odot$ is reached at magnitude V= 23.

paring their CMD to Baraffe et al. (1998) PMS evolutionary models, they identify a population of PMS stars with ages of $0.5 - 1.0$ Myr. Moreover, by adopting a set of MS isochrones from Lejeune & Schaerer (2001), they provide tentative hints of the presence of an evolved MS population of $2.0 - 2.5$ Myr. Note that this age estimate is based on the comparison of the MS isochrones with the position of three massive evolved O stars in their IR CMDs. Coupling this piece of evidence with the presence of the evolved post-red supergiant star Sher 25 (Moffat 1983) in the cluster field, HA08 hypothesize a possible age spread in the cluster population suggesting the presence of two distinct bursts in the star formation history, separated by ~ 10 Myr. It is interesting to note that recently Melena et al. (2008) have placed Sher 25 at the same distance as NGC 3603, suggesting a common origin.

The same ISAAC observations analyzed by HA08, were previously used by Stolte et al. (2004) and Brandl et al. (1999) to study the low-mass stars population in NGC 3603. While by inspecting the CMDs shown in their Figure 4 and 3c, respectively, signatures of the presence of a low MS population in the CMDs can not be ruled out, both these papers agree on dating a PMS population in the range of $0.5 - 1$ Myr.

SB04 published what was by then the deepest optical CMDs based on a combination of $UBVI$ and $H\alpha$ photometry from the Siding Spring Observatory (SSO) and archival HST/WFPC2 observations. The SSO ground-based CMDs sample the brightest massive population. The WFPC2 CMD samples stars down to $V \simeq 21$. In the very central region of the cluster ($r < 12''$), the CMD shows the presence of a well defined population of massive MS stars together with a population of low mass PMS objects. Apparently only few MS stars are detected in the cluster center at magnitudes fainter than $V \simeq 19.5$, while in the external regions ($18'' - 120''$) stars with masses down to $\sim 1 M_\odot$ are detected both in the MS and

PMS regions.

By using archival WFPC2 observations in the F656N band combined with the WFPC2 broad-band photometry, SB04 were able to identify objects with excess Hα emission, which is a signature of the PMS phase. While the majority of these objects on their CMD occupies a region consistent with very young PMS isochrones (1 Myr), some stars fall near the ZAMS (see their Figure 7). SB04 speculate on a possible spread in age of the cluster stars, but they warn that it is difficult to reach a firm conclusion because of the decreasing completeness and photometric accuracy of their photometry at fainter magnitudes ($V > 19$).

A careful examination and comparison of the recent studies on NGC 3603 mentioned above shows that they do not exclude the possible presence of multiple star formation episodes in the recent cluster history and even of a population of low mass MS stars. However, this scenario necessarily lacks a clear observational confirmation, since field contamination remains a crucial point in the study of stellar populations in NGC 3603. An efficient way to overcome these obstacles, when observations exist that are separated by a sufficiently large temporal baseline ($\geq 10 yr$), is the use of proper motions to separate cluster stars from foreground and background objects.

As mentioned in Section 3.1, the proper motions study for the core region of NGC 3603 by Rochau et al. (2010) showed signatures of at least two star formation epochs in the cluster, 1-2 Myr and 4-5 Myr old, respectively. Moreover, the CMD as cleaned-up from the field stars, reveals the presence of a low mass MS. The authors conclude that the latter is likely a population of objects not belonging to the cluster, that the proper motion technique failed to identify. We will offer later in our paper new observational evidence supporting the hypothesis that an old stellar population belonging to the cluster is present in the region of the CMD occupied by the candidate low MS stars identified by Rochau et al. (2010).

As an alternative and independent method to investigate the star formation history in NGC 3603, we have decided to take full advantage of our new deep $F656N$ band exposures to search for objects with excess Hα emission, since this feature is a good indicator of the PMS stage and therefore of recent star formation. By looking at the spatial distribution and age of all the objects with Hα excess emission, we will be able to better understand their cluster membership.

4. Hα EMISSION STARS

The presence of a strong Hα emission line ($EW_{H\alpha} \gtrsim 10$ Å) in young stellar objects is normally interpreted as a signature of the mass accretion process onto the surface of the object that requires the presence of an inner disk (see Feigelson & Montmerle 1999; White & Basri 2003, and reference therein).

The traditional approach to search photometrically for Hα emitters is based on the use of the R-band magnitude as a measure of the level of the photospheric continuum near the Hα line, so that stars with strong Hα emission will have a large $R-H\alpha$ color. However, as discussed in De Marchi et al. (2010a), since the R band is over an order of magnitude wider than the Hα filter, the R-Hα color does not provide an accurate measurement of the stellar continuum level inside the Hα band. Thus, while helpful to identify PMS stars, the $R-H\alpha$ color does not provide an absolute measure of the Hα luminosity nor of the Hα equivalent width. This additional information can be derived using measurements in the neigh-
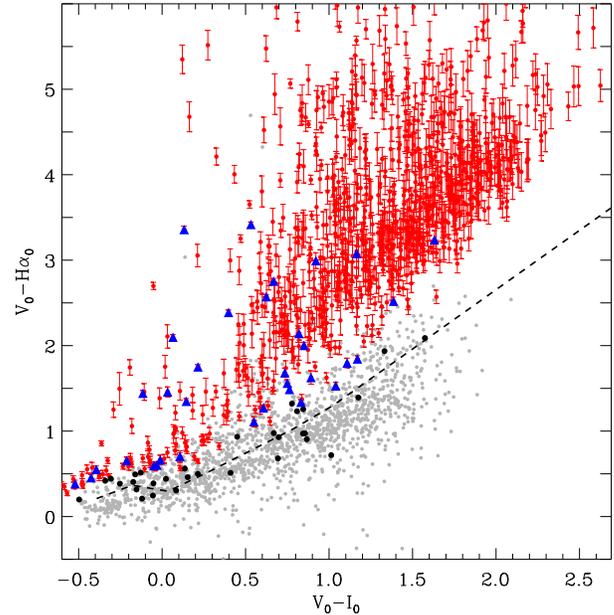

FIG. 4.— Selection of Hα emission excess stars in a color-color diagram. The dashed line represents the median $V-H\alpha$ color representative of stars with no Hα excess. Solid triangles and circles show the position on the diagram of the counterpart of the 67 objects with Hα excess emission by SB04 accepted and rejected through our selection criteria, respectively.

boring V and I bands, as recently shown by De Marchi et al. (2010a). This method allows us to reliably identify PMS objects actively undergoing mass accretion regardless of their age. Briefly, the method combines V and I broad-band photometry with narrow-band Hα imaging to identify all stars with excess Hα emission and to measure their Hα luminosity and mass accretion rate (see De Marchi et al. 2010a, for more details).

We followed this approach to select bona-fide PMS stars in the field of NGC 3603. Figure 4 shows the $V-H\alpha$ vs. $V-I$ diagram for the stars in our catalogue. We use the median $V-H\alpha$ dereddened color of stars with small (< 0.05 mag) photometric uncertainties in each of the three V, I and Hα bands, as a function of $V-I$, to define the reference template with respect to which the excess Hα emission is identified (dashed line in Figure 4). We selected a first sample of stars with excess Hα emission by considering all those with a $V-H\alpha$ color at least 5σ above that of the reference line, where σ here is the uncertainty on the $V-H\alpha$ color of the star. Then we calculated the equivalent width of the Hα emission line ($EW_{H\alpha}$) from the measured color excess using Equation 4 of De Marchi et al. (2010a). We finally considered as bona-fide PMS stars those objects with $EW_{H\alpha} > 10$ Å (White & Basri 2003) and $V-I > 0$; this allows us to clean our sample from possible contaminants, such as older stars with chromospheric activity and Ae/Be stars, respectively (see Scholz et al. 2007).

With this approach, we selected a first sample of ~ 800 objects with Hα excess emission. Through a visual inspection of the images, we noticed that some of these objects, although well detected both in the V and I bands, are located along filaments of gas and dust clearly visible in the Hα image (see right panel in Figure 1). It is crucial to consider that, if the centroid of a star falls on top of a filament that is only partially included in the annulus that our photometry routines use for background subtraction (from 4 to 7 pixel radius), the back-
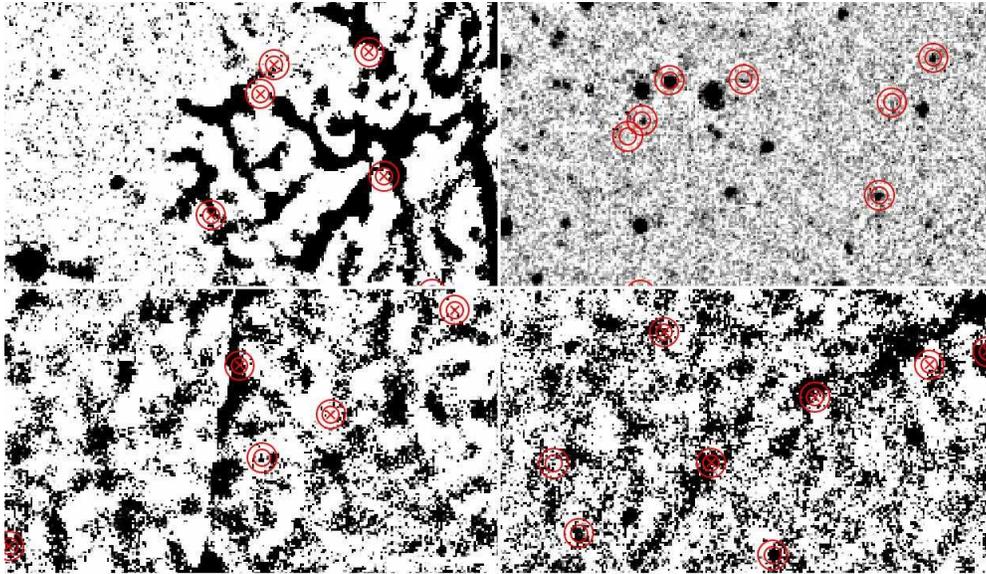
FIG. 5.— Four regions (each about 9" x 5" in size) of the drizzled Hα image as obtained by applying an unsharp-masking algorithm to highlight and sharpen the details of the dusty and cloudy structures. All candidate Hα excess emitters are marked with two concentric annuli (4 and 7 pixels radius, respectively). The objects excluded from our bona-fide sample are marked with a cross.

ground will be underestimated and the derived Hα magnitude of the star will be over estimated. All sources with Hα excess emission have been visually inspected and all those falling on top of one of such filaments conservatively excluded.

As an example, we show in Figure 5 four regions (each about 9" x 5" in size) of the drizzled Halpha image (with the highest spatial resolution and free of cosmic rays) as obtained by applying an unsharp-masking algorithm to highlight and sharpen the details of the gas filaments. All stars with apparent Hα excess emission are marked on the Figure with two concentric annuli corresponding to the area in which the background has been estimated (4 and 7 pixel radius, respectively). We have marked as suspicious and excluded from our bona-fide sample all those with significant and non-uniform filament contamination inside the photometric aperture (see objects marked with a cross in Figure 5). In this way, we reduced our sample to 412 objects with 5σ Hα excess emission that we consider bona-fide PMS stars.

In light of the considerable amount of differential reddening present in our field, one issue that needs to be taken into account is the impact that extinction will have on our selection of objects with Hα excess emission. Uncertainties on the extinction will move the objects in Figure 4, mostly along the $V-I$ axis, thereby changing the reference value of the $V-H\alpha$ color. In other words, variable extinction would change the reference relation (dashed line) to redder or bluer colors for individual stars. In order to estimate the impact of differential reddening, we have simulated the uncertainty introduced by a variation of ±0.2 mag in $E(V-I)$. According to SB04, such a value is the characteristic reddening variation seen in the area covered by our observations (see their Figure 5). Furthermore, it corresponds to $\Delta Av = \pm0.5$ mag, which fully covers this spread between the $Av = 5.5$ value that we find for the reddening and the canonical figure for NGC 3603 ($Av = 4.5$). If the true $E(V-I)$ value of a star were underestimated, we would also underestimate its $V-H\alpha$ excess, thereby in practice imposing a more stringent limit on the excess value itself. By underestimating $E(V-I)$ by 0.2 mag, our 5σ detection limit would correspond to about 6σ. Conversely, by overestimating the true $E(V-I)$ by 0.2 mag, about 17 % of the stars detected

at the 5σ level will drop below that, but all of them would still be above the 4σ level. Therefore, while there might be small uncertainties as to the value of the Hα excess for a specific object, the adoption of an average extinction value across the field does not significantly affect our selection of bona-fide PMS stars.

In Figure 6 we indicate with black dots the positions in the average dereddened CMD of all objects with excess Hα emission. The comparison with the theoretical 1, 3 and 10 Myr PMS isochrones of Siess et al. (2000) (dotted-dashed, solid and short-dashed line, respectively) suggests a typical age of $\sim 3\,Myr$ for 2/3 of the objects with Hα excess emission, but a surprising 1/3 of them are lying at or near the ZAMS (long dashed line), thus suggesting a considerably higher age, of order 20–30 Myr. A 10 Myr PMS isochrone seems to efficiently divide the stars with Hα excess emission in two populations, one lying near the ZAMS and the other in the PMS region.

Even though the fraction of PMS stars showing accretion is known to drop rapidly with age, Sicilia-Aguilar at al. (2010) recently found evidence of stars older than 10 Myr still undergoing mass accretion (see also Nguyen et al. 2009, and references therein). In the LMC, De Marchi et al. (2010a) found about 130 actively accreting PMS stars with a median age of 14 Myr indicating that ~ 10 Myr old stars can show Hα excess emission due to the accretion process.

However, as already discussed in Section 3.1, the region of the CMD fitted by the ZAMS track is strongly contaminated by field stars. It is then crucial to understand whether the objects with Hα excess emission that we see in NGC 3603 are indeed cluster members belonging to a previous generation or are just very young field stars. We will show in Section 5 the results of a statistical analysis of stellar membership providing convincing evidence that these older PMS stars have a different distribution from that of field objects.

It is known that one property of the accretion process that characterizes PMS stars is temporal variability, which can be traced to changes both in the continuum and more importantly in the emission lines (e.g. Herbst 1986; Hartigan et al. 1991; Nguyen et al. 2009). As mentioned in Section 3.2, SB04 published a list of sources with Hα emission in NGC 3603 de-
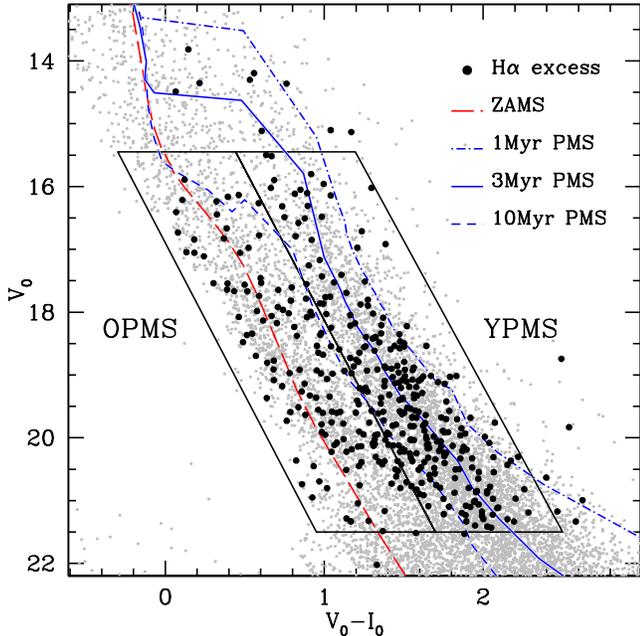
FIG. 6.— The location of stars with Hα excess (black points) are shown on the CMD together with a ZAMS and the 1, 3 and 10 Myr PMS isochrones adopted in Figure 3 (long dashed, dotted-dashed, solid and short-dashed line, respectively). As expected, most of the selected objects are young PMS stars (age < 10 Myr; YPMS box). Surprisingly, a number of sources are located on or near the ZAMS isochrone, i.e. in a position of the CMD compatible with a older PMS population (age > 10 Myr; OPMS box). The selection boxes of the two populations are shown (black lines).

rived from SSO and WFPC2 observations. We searched for the counterparts of these objects in our observations by cross-correlating our photometric catalogue with that of SB04. The stars detected by SB04 on the SSO data are bright and are all saturated in our images. On the other hand, the WFPC2 catalogue of SB04 contains 96 sources selected on the basis of their Hα index, of which 67 have a counterpart in our catalogue. As for the 29 missing objects, ten fall in the inner $10''$ of the cluster center, where saturation in our images makes star detection very difficult. Two of the remaining 19 sources fall outside the UVIS FoV, while the others are very close to the saturation limit in our catalogue or fall into the gaps of the UVIS mosaic.

All these 67 sources had Hα excess emission at the time of the SB04 observations, but only 35 of them have Hα excess emission at the $> 5\sigma$ level when our observations were taken. This number decreases to 23 if we consider only stars with $EW_{H\alpha} > 10$ Å. When lowering the threshold to 3σ, the number of stars with Hα excess in common with SB04 grows to 41, but only 25 of them have $EW_{H\alpha} > 10$ Å. This means that most ($\sim 65\%$) of the sources showing Hα excess in the study of SB04 (March 1999) do not show it at the epoch of our observations (Aug 2009). This is in line with the current understanding of the accretion mechanism whereby the in-falling material from the circumstellar disk is subject to bursts, corresponding to peaks in the Hα emission (e.g. Fernandez et al. 1995).

SB04 looked for matches between bright X-ray sources and objects with Hα excess emission by using archive Chandra X-Ray Observatory images. Only $\sim 1/3$ of the 96 Hα excess emission sources in the WFPC2 data set have a X-ray emission. We found that of the 23 stars with Hα excess emission in

common between our catalogue and that of SB04, a total of 8 have X-ray emission, according to SB04. While it is expected PMS stars actively undergoing mass accretion to be detected in X-rays, it is also true that the physical processes related to X-ray flaring and those pertaining to mass accretion are not the same (see e.g. Feigelson 2005). As shown by SB04, we should not expect a complete match between the sources that are bright in X rays and those showing Hα excess at any given time. And, obviously, even less so when the observations are not simultaneous, as in the case of the Chandra and HST data used by there authors, because of the considerable variability to which the accretion process is subject (see above).

5. SPATIAL DISTRIBUTION OF PMS STARS

The presence of stars with Hα excess emission overlapping the ZAMS in the CMD of Figure 6 offers new support to the hypothesis of a spread in the age of the PMS stars in NGC 3603 (see HA08 and references therein), since this is the region where PMS stars older than 10 Myr are expected to be located. One obvious issue to address is whether these objects are cluster members, as we know that there is a potentially significant contribution from field stars in this region (see Section 3.1). In order to investigate cluster membership for stars showing Hα emission, we can look at their spatial distribution compared to that of field stars.

Based on the distribution of Hα excess objects in the CMD, we define two regions containing bona-fide PMS stars (i.e. those with Hα excess of different ages). The 10 Myr PMS isochrone is used as a guide to define a rough separation between the young PMS population (< 10 Myr; hereafter YPMS) and the old PMS population (> 10 Myr; hereafter OPMS). We finally define as field population all stars lying in the OPMS box and not showing Hα excess. The corresponding selection areas are shown as boxes in Figure 6. It is important to underline here that, having defined as bona-fide PMS stars only the objects with excess Hα emission, we are in practice setting a lower limit to the actual number of stars in the PMS phase in NGC 3603, since some of them can be in the PMS stage without showing any Hα excess because of the variability of their Hα flux (see Section 4). This is certainly the case for the largest majority of stars that lie to the right of the 10 Myr isochrone in Figure 3. On the other hand, since we are interested in the radial distribution of PMS stars, selecting only objects with Hα excess emission does not affect the significance of our statistical analysis.

The cumulative radial distribution of the four groups defined above (PMS, YPMS, OPMS and Field) with respect to the cluster center is shown in the left panel of Figure 7, whereas in the right panel the positions of YPMS stars (crosses) and of OPMS stars (filled circles) are shown on the $F656N$ band image. To calculate the radial distribution of these objects we adopted the RA(J2000) = $11^{h} 15^{m} 7\overset{s}{.}26$ and DEC(J2000) = $-61° 15' 37\overset{''}{.}9$ as coordinates for the cluster center, following SB04. We exclude from our analysis the innermost $5''$ radius where there is a high concentration of bright O-B type stars that are saturated in our long exposures, and the high crowding level makes object detection difficult. The radius $r = 70''$ defines the largest circle inscribed in the FoV.

The graph on the left panel of Figure 7 clearly shows that PMS stars (solid line) are more centrally concentrated than field stars (dot-dashed line). Furthermore, the radial distributions of YPMS and OPMS stars (dotted and dashed lines, respectively) are clearly different from the field population,
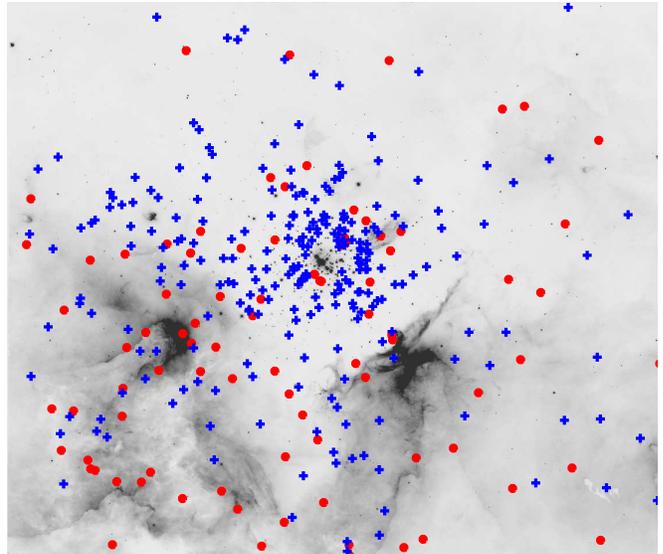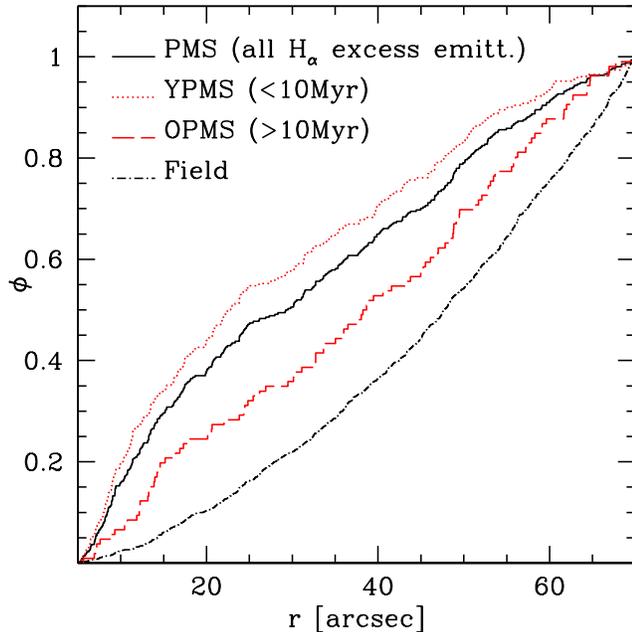
FIG. 7.— *Left panel*–Cumulative radial distribution of the four star groups as indicated in the legend. *Right panel*– The location of YPMS (crosses) and OPMS (solid circles) over-imposed on the *F656N* image already shown on Figure 1.

supporting the idea that these stars belong to NGC 3603. We used a Kolmogorov-Smirnov (KS) test to check the statistical significance of the differences in the observed distributions. The test yields more than 3σ confidence level that field stars have a different radial distribution from that of the PMS, YPMS and OPMS groups.

Interestingly, YPMS stars appear to be more centrally concentrated than OPMS objects, contrary to what one would expect in a triggered star formation scenario. Note that the KS test, as used here, indicates the probability that the different groups are drawn from the same population on the basis of their radial distribution with respect to a common center. In principle, however, the assumption of a common center of gravity for the PMS population as a whole could be incorrect, since the center of gravity of the OPMS stars might as well differ from that of the younger YPMS population. Nonetheless, the analysis presented here clearly shows how powerful the use of the Hα excess information can be to identify bona-fide PMS stars and to properly separate them from the field star population.

6. DISCUSSION AND CONCLUSIONS: THE STAR FORMATION HISTORY OF NGC 3603

The literature on the study of the stellar population of NGC 3603 offers a wide debate on the age of the stars in this cluster and on their formation history. While Stolte et al. (2004) and SB04 suggest 1 Myr as a common age for massive MS stars and PMS objects, possible evidence of larger age spreads comes from the analysis of the population of massive stars. HA08 derive an age of $2-2.5$ Myr for MS stars through isochrone fitting of three massive stars in the center of the cluster classified as WN6h+abs objects by Crowther & Dessart (1998), while they date the PMS stars in the range $0.5-1.0$ Myr. Hendry et al. (2008) also notice that the massive-star population in NGC 3603 appears to be predominantly coeval (with an age of $1-2$ Myr), but that Sher 25, and one O-type supergiant, are likely to be slightly older ($\sim$4-5 Myr; Melena et al. 2008; Crowther et al. 2006).

Sher 25 (Sher 1965; Moffat 1983) is clearly visible in Figure 1 and has been recently classified as a blue supergiant (BSG) surrounded by an asymmetric, hourglass-shaped circumstellar nebula by Hendry et al. (2008).

HA08 suggests the possibility that, if Sher 25 belongs to the cluster, two distinct star formation episodes separated by ~ 10 Myr should be present in NGC 3603. Sher 25 is not the only BSG in the NGC 3603 region. Spectroscopy by Moffat (1983) revealed two other BSGs in the vicinity of the cluster core (see also Figure 1 from Brandner et al. 1997). The latter authors conclude that the simultaneous presence of BSGs and stars of MK type O3 V requires at least two distinct episodes of star formation in NGC 3603 separated by ~ 10 Myr.

Our study shows that the OPMS population belongs to NGC 3603 and not to the field, thus establishing unambiguously for the first time that the star formation of this cluster is not characterized by a 1-2 Myr single burst. These objects might indeed represent the low mass population of a star formation episode that occurred more than 10 Myr ago, which would naturally explain the presence in the same region of evolved massive stars (age > 10 Myr) like Sher 25.

In order to better understand how star formation has proceeded recently in NGC 3603, we can look at the age distribution of PMS stars in the CMD. Shown in the left panel of Figure 8 are the PMS isochrones of Siess et al. (2000) for ages of 1, 2, 4, 8, 16, 32 and 64 Myr. Note that the photometric uncertainty of our data (see large crosses on the figure) confirms that it is possible to assign relative ages to these stars with an accuracy of better than a factor of 2. Solid thick points and asterisks in the figure represent all bona-fide PMS objects (i.e. those with Hα excess emission) having ages in the range $1-64$ Myr and masses between 0.9 and $4\,M_\odot$. The corresponding age distribution is shown by the solid histogram in the right panel of the figure. In the same panel we also show, as a dashed line, the histogram of the age distribution of all stars with no Hα excess younger than 16 Myr and with masses in the range from 0.9 and $4\,M_\odot$, marked as small dots in the
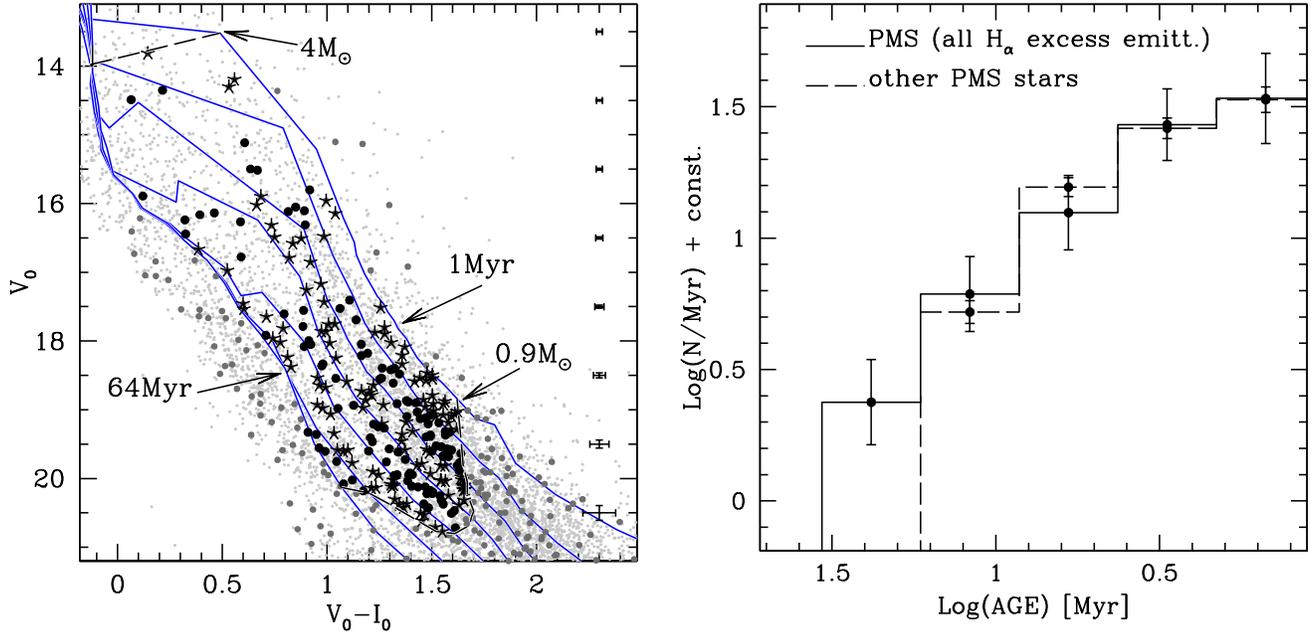
FIG. 8.— *Left panel–* CMD showing the position of Hα stars (solid points and asterisks) together with the 1, 2, 4, 8, 16, 32 and 64 Myr isochrones from Siess et al. (2000) used to assign the age to the stars in the range of masses between 0.9 and 4 $M_\odot$. PMS stars as counted in different age intervals are shown as thick dark dots and asterisks, alternatively. The other PMS stars are shown with large grey dots, whereas all other cluster stars are shown with smaller grey points. *Right panel–* Histogram of the number of PMS stars (i.e. stars showing Hα excess emission) per Myr as a function of age (solid line). The same histogram for all other stars is shown for comparison (dashed line). Note that for the these stars we have only sampled the age distribution up to 16 Myr, in order to avoid the significant field star contamination in the bluest part of the CMD.

left-hand panel (note that the few remaining bona-fide PMS stars outside of these age and mass ranges, shown as thick grey points, and are not considered here). For the objects with no Hα excess emission we have only sampled the age distribution younger than 16 Myr, in order to avoid the significant field star contamination in the bluest part of the CMD. For comparison purposes, their histogram has been normalized vertically (i.e. shifted by 1.1 dex) so as to match the distribution of the bona-fide PMS stars at the youngest age.

The histograms of Figure 8 show that star formation in NGC 3603 has been ongoing for at least 10–20 Myr and no gaps are evident, at least at the level of resolution that we have adopted for the age (a factor of two, as shown by the size of the bins). If we consider stars with no Hα excess emission, for which no selection effects are present other than photometric completeness that is nonetheless always > 85 %, we would have to conclude that over the past ∼ 16 Myr the star formation rate in this region has been progressively increasing. However, it is important to consider that many of the older stars might have migrated out of our FoV. According to Rochau et al. (2010), the velocity dispersion of stars in the central regions of NGC 3603 is ∼ 4.5 km s^{-1} and appears to be pretty constant in the mass range that they sample (∼ 1.7−9$M_\odot$). This implies that a 10 Myr old star would have had time to travel as far as 45 pc away from its birthplace, i.e. well beyond the ∼ 5 × 5 pc^2 area covered by our observations. This might be one of the causes of the observed drop in the number of stars with increasing age shown in the histogram of Figure 8, and would also explain the somewhat different radial distributions of old and young PMS stars seen in Figure 7. A survey of a wider area around NGC 3603 is needed to properly address the evolution of the star formation rate in this cluster.

Interestingly, the age distribution of bona-fide PMS stars

does not seem to differ in any systematic way within the error bars from that of objects with no Hα excess, seemingly suggesting that the ratio of PMS stars with and without Hα excess emission is not a function of age. This might appear at odds with common wisdom suggesting that the efficiency of the accretion process at the origin of the Hα emission should decrease with time as a PMS objects approaches the MS (see Sicilia-Aguilar at al. 2010; De Marchi et al. 2010a, and references therein). However, selection effects here can be important. In particular, as PMS objects approach the MS, both their Hα and bolometric luminosities decrease, but not necessarily in the same way. If the bolometric luminosity drops more rapidly than the Hα luminosity, PMS stars of older ages will become easier to identify for our method since it requires an excess emission at the 5 σ level or higher (see De Marchi et al. 2010a).

This effect can have important implications on our understanding of the accretion process and of the star formation rate, which we will address in a forthcoming paper comparing the star formation process in a number of young clusters. We have already started to study the stellar population in the 30 Doradus region in the LMC, applying the same observational strategy described in this work, and using the recently released WFC3 observations of this region. By searching for objects with Hα excess emission, we have already found tantalizing evidence of multiple star formation episodes (De Marchi et al., in preparation), like in NGC 3603. Furthermore, two distinct populations with ages of ∼ 1 and ∼ 15 Myr are present in the population of the star cluster NGC 346 in the Small Magellanic Cloud (De Marchi et al., in preparation). Given the different environmental conditions and chemical compositions of the three clusters ($Z_\odot$ for NGC 3603, ∼ 1/3 $Z_\odot$ for 30 Dor and ∼ 1/10 $Z_\odot$ for NGC 346; see HA08, Andersen et al. 2009 and Hennekemper et al. 2008, respec-

tively), this similarity supports the hypothesis that continuing star formation could be the preferential channel for the formation of stars in starburst clusters.

According to Vinkó et al. (2009), the young cluster Sandage 96 in NGC 2403 is known to positively exhibit a young population ($10-16$ Myr) together with a relatively old one ($32-100$ Myr) thus suggesting multiple star formation events in a range of ages at least 4 times wider than in NGC 3603. A spread in the MS turn-off has been reported for clusters of intermediate age in the LMC and has been interpreted as an age spread of ~ 300 Myr (see Milone et al. 2009). Moreover, the discovery of multiple stellar populations along the MS and red giant branch of a large number of Galactic globular clusters (Piotto 2008; Lee et al. 2009) requires two or more bursts in the star formation history of these objects, separated by at least few 10^7 yr (see Carretta et al. 2010, and references therein).

Therefore, it appears that multiple generations of stars spread over a wide range of ages are present in star clusters. A detailed investigation will be necessary in order to understand what is at the origin of the observed age spread and, for example, what is the influence of the environment and chemical/physical state (metallicity, turbulence, density, mass, etc.)

of the parent molecular cloud on the formation of stars in clusters.

Establishing whether age spreads like those seen in NGC 3603 are common in starburst clusters will have profound implications for theories of star cluster formation, for the meaning and determination of the IMF and finally for the general assumption that clusters are simple stellar populations.

REFERENCES

Alencar, S. H. P., & Batalha, C. 2002, ApJ, 571, 378
Alencar, S. H. P., Basri, G., Hartmann, L., & Calvet, N. 2005, A&A, 440, 595
Andersen, M., Zinnecker, H., Moneti, A., McCaughrean, M. J., Brandl, B., Brandner, W., Meylan, G., & Hunter, D. 2009, ApJ, 707, 1347
Appenzeller, I., & Mundt, R. 1989, A&A Rev., 1, 291
Ascenso, J., Alves, J., Beletsky, Y., & Lago, M. T. V. T. 2007, A&A, 466, 137
Baraffe, Chabrier, Allard, Hauschildt, 1998, A&A, 337, 403
Batalha, C., Lopes, D. F., & Batalha, N. M. 2001, ApJ, 548, 377
Baumgardt, H., & Kroupa, P. 2007, MNRAS, 380, 1589
Bertout, C. 1989, ARA&A, 27, 351
Brandl, B., Brandner, W., Eisenhauer, F., Moffat, A. F. J., Palla, F., & Zinnecker, H. 1999, A&A, 352, L69
Brandner, W., Grebel, E. K., Chu, Y.-H., & Weis, K. 1997, ApJ, 475, L45
Cardelli, J. A., Clayton, G. C., & Mathis, J. S. 1989, ApJ, 345, 245
Carretta, E., Bragaglia, A., Gratton, R., Recio-Blanco, A., Lucatello, S., D'Orazi, V., & Cassisi, S. 2010, arXiv:1003.1723
Cool, A. M., Piotto, G., & King, I. R. 1996, ApJ, 468, 655
Crowther, P. A., Lennon, D. J., Walborn, N. R., & Smartt, 2006, arXiv:astro-ph/0606717
Crowther, P. A., & Dessart, L. 1998, MNRAS, 296, 622
De Marchi, G., Panagia, N., & Romaniello, M. 2010, ApJ, in press (arXiv:1002.4864)
Feigelson, E.D., & Montmerle, T. 1999, Ann. Rev. å37, 363
Feigelson, E. D. 2005, 13th Cambridge Workshop on Cool Stars, Stellar Systems and the Sun, 560, 175
Fernandez, M., Ortiz, E., Eiroa, C., & Miranda, L. F. 1995, A&AS, 114, 439
Grebel, E. K. 2004, The Formation and Evolution of Massive Young Star Clusters, 322, 101
Harayama, Y., Eisenhauer, F., & Martins, F. 2008, ApJ, 675, 1319 (HA08)
Hartigan, P., Kenyon, S. J., Hartmann, L., Strom, S. E., Edwards, S., Welty, A. D., & Stauffer, J. 1991, ApJ, 382, 617
Hendry, M. A., Smartt, S. J., Skillman, E. D., Evans, C. J., Trundle, C., Lennon, D. J., Crowther, P. A., & Hunter, I. 2008, MNRAS, 388, 1127
Hennekemper, E., Gouliermis, D. A., Henning, T., Brandner, W., & Dolphin, A. E. 2008, ApJ, 672, 914
Herbst, W. 1986, PASP, 98, 1088
Johns, C. M., & Basri, G. 1995, AJ, 109, 2800
Jones, T. J., Ashley, M., Hyland, A. R., & Ruelas-Mayorga, A. 1981, MNRAS, 197, 413
Kalirai, J. S., et al. 2009, Instrument Science Report WFC3 2009-31, 27 pages, 21

Kozhurina-Platais, V., Cox, C., McLean, B., Petro, L., Dressel, L., Bushouse, H., Sabbi,E. 2009, Instrument Science Report WFC3 2009-33, 22 pages, 33
Kurucz, R. L. 1993, IAU Colloq. 138: Peculiar versus Normal Phenomena in A-type and Related Stars, 44, 87
Larsen, S. S. 2009, A&A, 494, 539
Lee, J.-W., Kang, Y.-W., Lee, J., Lee, Y.-W. 2009, Nature, 462, 480
Lejeune, T., & Schaerer, D. 2001, A&A, 366, 538
Marigo, P., Girardi, L., Bressan, A., Groenewegen, M. A. T., Silva, L., & Granato, G. L. 2008, A&A, 482, 883
Mayne, N.J., & and Naylor, T. 2008, MNRAS 386, 261
Melena, N. W., Massey, P., Morrell, N. I., & Zangari, A. M. 2008, AJ, 135, 878
Milone, A. P., Bedin, L. R., Piotto, G., & Anderson, J. 2009, A&A, 497, 755
Moeckel, N., & Bate, M. R. 2010, arXiv:1001.3417
Moffat, A. F. J. 1983, A&A, 124, 273
Nguyen, D. C., Scholz, A., van Kerkwijk, M. H., Jayawardhana, R., & Brandeker, A. 2009, ApJ, 694, L153
Nürnberger, D. E. A., & Petr-Gotzens, M. G. 2002, A&A, 382, 537
Palla, F., & Stahler, S. W. 1999, ApJ, 525, 772
Peters, T., Banerjee, R., Klessen, R. S., Mac Low, M.-M., Galvan- Madrid, R., & Keto, E. 2010, arXiv:1001.2470
Piotto, G., Zoccali, M., King, I. R., Djorgovski, S. G., Sosin, C., Rich, R. M., & Meylan, G. 1999, AJ, 118, 1727
Piotto, G. 2008, Memorie della Societa Astronomica Italiana, 79, 334
Portegies Zwart, S., McMillan, S., & Gieles, M. 2010, arXiv:1002.1961
Robin, A. C., Reylé, C., Derrière, S., & Picaud, S. 2003, A&A, 409, 523
Rochau, B., Brandner, W., Stolte, A., Gennaro, M., Gouliermis, D., Da Rio, N., Dzyurkevich, N., & Henning, T. 2010, ApJ, 716, L90
Scholz, A., Coffey, J., Brandeker, A., & Jayawardhana, R. 2007, ApJ, 662, 1254
Sicilia-Aguilar, A., Henning, T., Hartmann, L. W. 2010, ApJ, 710, 597
Siess, L., Dufour, E., & Forestini, M. 2000, A&A, 358, 593
Stetson, P. B. 1987, PASP, 99, 191
Stetson, P. B. 1994, PASP, 106, 250
Stolte, A., Brandner, W., Brandl, B., Zinnecker, H., & Grebel, E. K. 2004, AJ, 128, 765
Stolte, A., Brandner, W., Brandl, B., & Zinnecker, H. 2006, AJ, 132, 253
Sung, H., & Bessell, M. S. 2004, AJ, 127, 1014 (SB04)
Symposium, 246, 181
Vinkó, J., et al. 2009, ApJ, 695, 619
White, R.J., & Basri, G. 2003, ApJ, 582, 1109
Wong, M.H., Pavlovsky, C., and Long, K. et al., 2010. ÒWide Field Camera 3 Instrument Handbook, Version 2.0Ó (Baltimore: STScI)